A Differentially Driven Flapping Wing Mechanism for Force Analysis and Trajectory Optimization

Ryan B. George, Mark B. Colton, Christopher A. Mattson and Scott L. Thomson
Brigham Young University, Ira A. Fulton College of Engineering and Technology, Department of Mechanical Engineering, 435 CTB, Provo, UT 84602, USA

ABSTRACT
Flapping flight has the potential to revolutionize micro air vehicles (MAVs) due to increased aerodynamic performance, improved maneuverability, and hover capabilities. This paper presents the design of a robotic flapping wing mechanism for use in general studies involving flapping flight and laboratory-based experimental optimization of flapping trajectories. The design allows for dynamic adjustment of flapping trajectories in air or liquids with three rotational degrees of freedom on each wing. The design, instrumentation, and control of the mechanism are discussed, and experimental characterization of the mechanism's performance is presented. Preliminary trajectory optimization using a Box-Behnken design approach is used and shows successful parameter optimization. The limitations of the current mechanism are addressed. A survey of flapping mechanisms is presented.

1. INTRODUCTION
Flapping-wing micro air vehicles (MAVs) may exhibit considerable advantages over fixed-wing and rotor-based MAVs due to the better aerodynamic performance, maneuverability, and hover capabilities that flapping flight makes possible [1]. Two specific lift generating mechanisms of flapping flight hold much promise for MAV design. The first is the clap-and-fling mechanism at the top (and sometimes bottom) of the flapping stroke, in which the two wings clap together and fling apart, creating a strong low-pressure zone between the wings; the second is the leading edge vortex (LEV) created by dynamic stall during flapping [2]. The versatile flapping mechanism that is presented in this paper, which is computer controlled and instrumented to measure flapping motion and wing forces, will enable investigations of these and other lift-generating mechanisms. The mechanism is also well suited for experimental optimization of flapping trajectories. This paper also presents preliminary optimization results based on the Box-Behnken screening design to select flapping trajectory parameters. The Box-Behnken screening design explores the design space in a manner similar to a factorial design, but is more efficient by excluding higher order interactions. This allows the optimization to sample a large design space with relatively few runs.

1.1 Background
The study of flapping flight from an experimental standpoint can bring insight into the lift-generating mechanisms produced during flapping. Developing our understanding of flapping-wing kinematics will enable the advancement of MAV technology and may contribute to a stronger understanding of biological organisms capable of flapping flight.

Although many flapping wing mechanisms currently exist, there is a need for an independently controlled dual-wing flapping mechanism that allows input of any user-specified trajectory, can be controlled from a remote location, has a wide range of motion, and is capable of measuring lift and thrust. The mechanism presented in this paper meets these specifications, and will serve as a test bed for flapping kinematic optimization and exploration of flapping flight for potential use in MAVs.

In this paper the theory and design of such a flapping mechanism is presented and preliminary force measurements and trajectory optimization results are presented.

1.2 Related Work

Much has been learned from previous experiments using flapping-wing mechanisms. Researchers at many institutions have designed flapping mechanisms that are wide-ranging in terms of purpose, function, appearance, and performance. Although these mechanisms do not have the complete functionality required for experimental optimization of flapping trajectories and studies of lift-generating mechanisms, they are worth mentioning and have influenced the design approach taken in this research. Table 1 contains a list of many of the notable flapping mechanisms. In this table "Adjustable Kinematics" refers to the mechanism controller's ability to change the flapping trajectory; "Operating Medium" refers to the fluid (air or liquid) in which the mechanism was designed to operate; "Setup" refers to the mechanism's ability to fly on its own; and "Purpose" refers to the types of experiments or other activities that the mechanism was designed to achieve.

Table 1. A survey of flapping wing mechanisms. List is organized chronologically, by date, and then alphabetically, by author.

	Adjustable kinematics		Operating Medium		Device Setup		Purpose		
Name	Yes	No	Air	Liquid	Fixed	Un-tethered	Flow viz/PIV	Force Analysis	Flight
Smith (1996)[3], Smith (2001)[4]	✓		✓		✓	✓		✓	✓
Van den Berg (1997)[5], Ellington (1999)[6]	✓		✓		✓		✓		
Dickinson (1999)[7]	✓			✓	✓			✓	
Fearing (2000)[8], Sitti (2001)[9]	✓		✓		✓			✓	
Frampton (2000)[10]		✓	✓		✓			✓	
Pornsin-Sisirak (2000)[11]		✓	✓			✓			✓
Yan (2001)[12]	✓		✓			✓		✓	✓
Cox (2002)[13]	✓		✓		✓			✓	
Avadhanula (2003)[14], Yan (2003)[15]	✓		✓			✓		✓	✓
Raney (2003)[16]	✓		✓		✓			✓	
Tarascio (2003)[17], Singh (2008)[18]		✓	✓		✓			✓	
Burgess (2004)[19]		✓	✓		✓			✓	
Mankame (2004)[20]		✓	✓		✓	✓		✓	✓
Maybury (2004)[21]	✓		✓		✓			✓	
Thomas (2004)[22]		✓	✓		✓		✓		
Banala (2005)[23]		✓	✓		✓			✓	
Galinski (2005)[24], Zbikowski (2005)[25]		✓	✓		✓		✓	✓	
Lai (2005)[26]	✓			✓	✓			✓	
Madangopal (2005, 2006)[27],[28]		✓	✓		✓	✓		✓	✓
McIntosh (2005)[29], Agrawal (2010)[30]		✓	✓			✓		✓	
Tanaka (2005)[31]		✓	✓		✓	✓	✓		✓
Yamamoto (2005)[32]		✓	✓		✓			✓	
Conn (2006, 2007)[33],[34]	✓		✓		✓			✓	
Issac (2006)[35]	✓			✓	✓			✓	

(continued)

	Adjustable kinematics		Operating Medium		Device Setup		Purpose		
Name	Yes	No	Air	Liquid	Fixed	Un-tethered	Flow viz/PIV	Force Analysis	Flight
Syaifuddin (2006)[36], Nguyen (2008)[37]	✓		✓			✓	✓	✓	✓
DiLeo (2007)[38]	✓			✓	✓			✓	
Khan (2007)[39]		✓	✓		✓			✓	
Wood (2007)[40]	✓		✓		✓	✓		✓	✓
Yang (2007)[41]		✓	✓			✓		✓	✓
Bunget (2008)[42]		✓	✓		✓		✓		
Grand (2008)[43]		✓	✓			✓			✓
Lentink (2008)[44]		✓		✓	✓		✓		
Maglasang (2008)[45]		✓	✓		✓		✓	✓	
Nagai (2008)[46]	✓			✓	✓			✓	
Park (2008)[47]		✓	✓			✓			✓
Bejgerowski (2009)[48]		✓	✓			✓		✓	✓
Bolsman (2009)[49]	✓		✓		✓			✓	
Finio (2009)[50]	✓		✓			✓			✓
Hubel (2009)[51]		✓	✓		✓		✓	✓	
Krashanitsa (2009)[52]		✓	✓			✓		✓	✓
Massey (2009)[53]		✓	✓		✓		✓	✓	
Thomson (2009)[54]	✓			✓	✓			✓	
Tsai (2009)[55]		✓	✓			✓		✓	✓
Fenelon (2010)[56]	✓		✓		✓			✓	
Han (2010)[57]		✓		✓	✓		✓	✓	
Mukherjee (2010)[58]	✓		✓		✓	✓		✓	✓

Some of the mechanisms listed in Table 1 are similar in design to the mechanism presented in this paper. Van den Berg and Ellington [5] created a flapping mechanism based on a differential design called "The Flapper." This mechanism was designed for use in air and, although this mechanism is capable of adjustable kinematics, the wings cannot flap independently. Dickinson and Sane [7] and DiLeo and Deng [38] both built mechanisms based on a robotic wrist mechanism. This design allowed a large range of motion while still keeping critical components out of the water. Lai et al. [26] introduced a mechanism also based on a differential gear design and used timing belts to drive each of the two inputs of the differential. The rotation angle used a turntable that did not allow for two wings.

The mechanism design presented in this paper has adjustable kinematics, can operate in water, oil, or air, is fixed, and can be used for flow visualization, particle image velocimetry (PIV), and force analysis. Although certain of the above mechanisms do meet these same functional criteria, they either do not have precision control using encoder feedback or do not have two wings to enable simulation of clap-and-fling.

2. SYSTEM DESIGN

A six-degree-of-freedom (6-DOF) flapping mechanism capable of executing arbitrary flapping trajectories was developed to explore the relationship between flapping trajectory, resulting wing forces, and flow patterns. Each wing was designed to have 3 DOFs, as shown in Figure 1. Rotation by θ_1 about the z-axis is referred to as the *rotation angle*; rotation by θ_2 about the y-axis is referred to as the *elevation angle*; and rotation by θ_3 about the x-axis is referred to as the *feathering angle*. To enable exploration of a wide range of flapping motions, the mechanism was designed to enable motions of $\theta_1 = \pm 90°$, $\theta_2 = +55/-105°$, and $\theta_3 = \pm 180°$ (based on the mechanical limits of the mechanism). With 3 DOFs per wing, the mechanism is capable of generating arbitrary flapping patterns to explore lift and

thrust generation. The optimization method presented in Section 3.2 and Section 4 is designed to find the trajectories that will maximize weighted combinations of lift and thrust to achieve the desired type of flight (hover, forward translation, hover and translation, etc.). The mechanism was designed to flap at a maximum frequency of 0.667 Hz, as defined by the trajectories described in Section 3.1. The design minimized gear backlash, and was designed for ease of setup and use, interchangeability of wing shapes and materials, and for interfacing with software for convenient implementation of new trajectories and optimization schemes. The mechanism is capable of measuring lift and thrust in water, oil, or air.

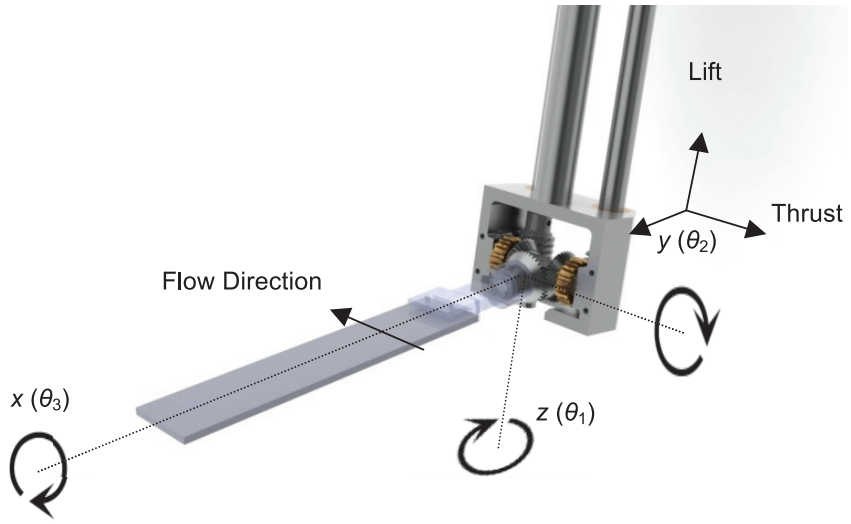

Figure 1. Coordinate definitions for the flapping wing mechanism, shown on the mechanism's right wing. The lift and thrust forces are aligned with inertial axes.

2.1 Mechanism Design

The design of the flapping mechanism is based on a differential gear model similar to the design by Van den Berg et al. [5] and Lai et al. [26]. Differentials transfer torque and rotational motion and are most commonly used in one of two ways. The first is one rotational input to generate two rotational outputs; the second is two inputs that create an output that is the sum, difference, or average of the inputs, depending on their speed and direction. The present design utilizes the latter approach to allow control of two output DOFs (θ_2 and θ_3) using motors mounted well above the differential, to prevent damage to the motors from the water or oil in which experiments are conducted. The third DOF (θ_1) is achieved by rotating the entire differential about its z-axis.

The mechanism includes a differential assembly housed inside a frame, as shown in Figure 2. Spur gears are mounted on the two input-differential gears. These spur gears are driven by worm gears mounted directly behind the spur gear to keep the design compact (Figure 3). The worm gears are mounted to long shafts that extend upwards out of the working fluid. Motors are directly mounted to the worm gear shaft to drive the two differential inputs (Figure 4).

The third DOF is accomplished using a turntable mounted above and directly in line with the longitudinal axis of the mechanism. The turntable contains gear teeth that interface with a gear attached to the shaft of a motor mounted in the same plane.

Two identical mechanisms are arranged back-to-back on a plate. For the study mentioned here, the plate was mounted to slotted framing which sits atop a water flume.

This design was chosen after careful consideration of other designs, which did not provide adjustable kinematics, did not have encoder feedback for trajectory control, or did not meet the design requirements for the desired tests. The proposed model allowed for adjustable kinematics, was capable of being submerged in water, and had two wings that allow for the exploration of clap and fling. The system was modeled using SolidWorks. All gears, bearings, pins, and clips were off-the-shelf components. All other parts were custom designed and toleranced.

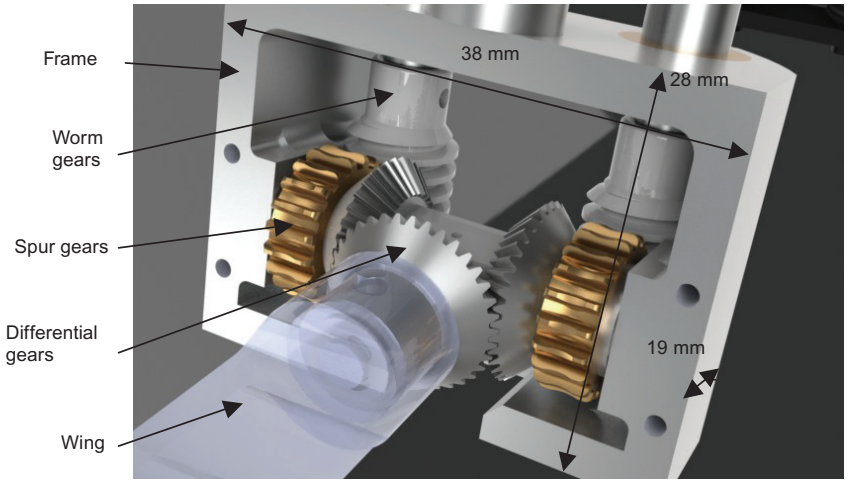

Figure 2. Differential and frame assembly. The frame is supported from above and the wing attaches to the output of the differential.

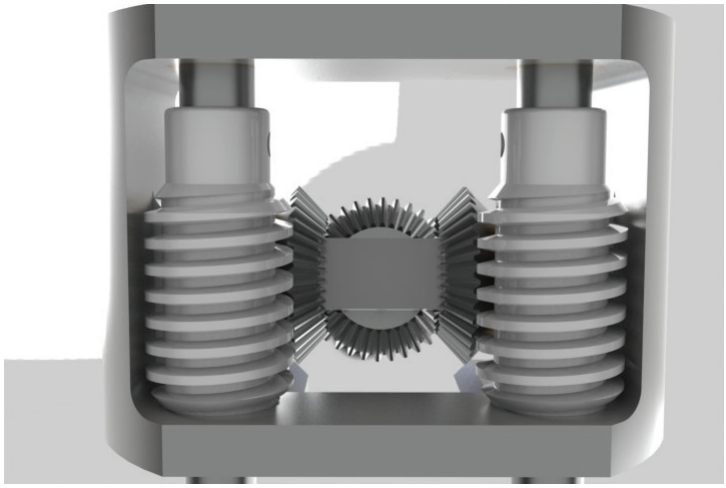

Figure 3. Rear view of housing and differential. Worm gears are located directly behind the two differential inputs for compact design.

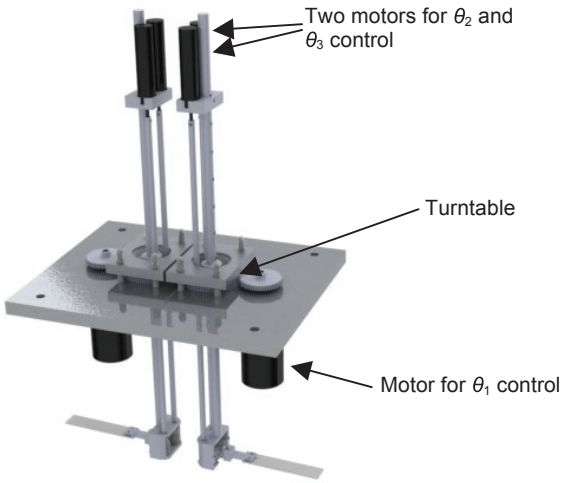

Figure 4. Motors mounted to the top of the mechanism on a turntable for θ_1 rotation.

2.2 Actuation and Control

Each DOF was actuated by brushless DC motors with integrated incremental encoders for position feedback and force-vector resolution. The θ_1 DOF was driven by a Maxon motor (part number EC 40-118899) with a stall torque of 363 mN·m, no-load speed of 3100 rpm, and integrated 500 count-per-turn encoder. The θ_2 and θ_3 DOFs were driven by identical Maxon motors (part number EC 16-232241) with a stall torque of 184 mN·m, no-load speed of 41400 rpm, and integrated 512 count-per-turn encoders. All six motors were driven by Advanced Motion Controls BE15A8 PWM servo drives that receive analog voltage commands from the controller.

A six-channel controller was developed to enable the flapping mechanism to track the desired angle trajectories $\theta_{1d}(t)$, $\theta_{2d}(t)$, and $\theta_{3d}(t)$ for each wing (where the subscript *d* denotes the desired angle). The controller was developed in LabVIEW and implemented on a National Instruments (NI) CompactRIO Real-Time Controller (cRIO-9074) augmented with an NI 9263 analog output module (for generating motor command voltages), an NI 9237 bridge module (for reading strain gage outputs), and an NI 9411 digital input module (for reading the encoders). Six independent PID controllers running at a rate of 500 Hz were implemented on the FPGA layer of the cRIO. The PID gains were tuned experimentally to ensure stability and satisfactory trajectory tracking in air and water. The FPGA layer also handled all sensor and motor I/O and communication with the PC layer, and the PC layer generated the desired trajectories using MATLAB.

2.3 Instrumentation

The objective of the mechanism's instrumentation is to measure the flapping angles ($\theta_1(t)$, $\theta_2(t)$, and $\theta_3(t)$), the lift force (f_L), and the thrust force (f_T) as the mechanism executes specified flapping trajectories. As mentioned previously, the flapping angles are sensed using encoders attached to the motors and recorded using the digital module of the cRIO. The resultant force vector on the wing is measured using four waterproofed strain gages [59] affixed to a wing bracket at the base of the wing (see Figure 5). The gages are connected in a full-bridge configuration, the output of which is conditioned using the bridge module of the cRIO. The force thus obtained is the force vector exerted on the wing and expressed in the wing-fixed coordinate frame. The objective of this work is to find flapping trajectories that maximize lift and thrust forces, which, by definition for a stationary, horizontally oriented body, are defined in the earth-fixed vertical (*z*) and forward (*y*) directions, respectively. It is therefore necessary to transform the force vector measured in the wing-fixed frame into the earth-fixed frame. This is accomplished by a 3-2-1 Euler angle transformation in which the axes are first rotated by angle θ_1 about the vertical axis, followed by a rotation by angle θ_2 about the horizontal shaft axis, followed by a rotation by angle θ_3 about the wing axis. The resulting rotation matrix is given by

$$R(\theta_3,\theta_2,\theta_1)=\begin{bmatrix}1&0&0\\0&\cos\theta_3&-\sin\theta_3\\0&\sin\theta_3&\cos\theta_3\end{bmatrix}\begin{bmatrix}\cos\theta_2&0&\sin\theta_2\\0&1&0\\-\sin\theta_2&0&\cos\theta_2\end{bmatrix}\begin{bmatrix}\cos\theta_1&\sin\theta_1&0\\-\sin\theta_1&\cos\theta_1&0\\0&0&1\end{bmatrix}. \quad (1)$$

The force expressed in the earth-fixed frame can then be found from the single component of force measured in the wing-fixed frame using

$$F_{earth}=R(\theta_3,\theta_2,\theta_1)^T F_{wing}. \quad (2)$$

As shown in Figure 1, the *y*-component of F_{earth} contains the thrust force and the *z*-component contains the negative lift force.

The angles used in the transformation, [θ_1, θ_2, θ_3], are measured in real-time using the motor encoders, as described previously. Because the center of pressure is constantly changing throughout the flapping cycle, a bending moment force sensor such as that currently employed on this mechanism is not capable of resolving lift and thrust forces in the units of force [7]. To eliminate any potential for errors due to the constantly shifting center of pressure, force values are left in arbitrary units (au) to properly compare them against each other.

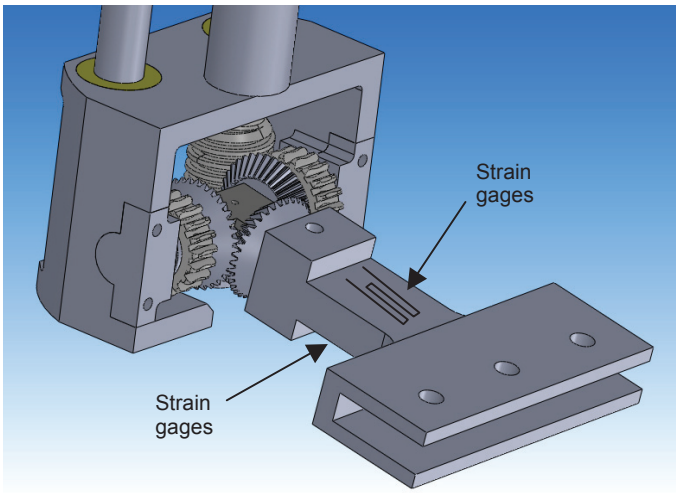

Figure 5. Strain gages fixed to a wing mounting bracket.

3. METHODS

To test the flapping mechanism, a structure was built to place the flapping mechanism in the center of a flume measuring 1.2 m wide, 0.33 m deep, and 10 m long. The structure allowed the flapping mechanism to be placed securely at any position along the flume length. Width and length adjustments could be made to place the mechanism in any position, while the depth adjustment was only allowed in discrete steps of 0.025 m (1 in). Flume water velocity was set to 0.25 m/s.

3.1 Wing Trajectories

The desired flapping trajectories were defined using the first five terms of a Fourier series expansion for each degree of freedom,

$$\begin{aligned}\theta_1(t) &= A_{11} + A_{12}\sin\omega t + A_{13}\cos\omega t + A_{14}\sin 2\omega t + A_{15}\cos 2\omega t \\ \theta_2(t) &= A_{21} + A_{22}\sin\omega t + A_{23}\cos\omega t + A_{24}\sin 2\omega t + A_{25}\cos 2\omega t \\ \theta_3(t) &= A_{31} + A_{32}\sin\omega t + A_{33}\cos\omega t + A_{34}\sin 2\omega t + A_{35}\cos 2\omega t\end{aligned}, \tag{3}$$

where A_{11} through A_{35} are the coefficients for each term, ω is the desired flapping frequency, and t is time. This is similar to the approach employed by Aono et al. [60], [61] but with fewer terms. It is acknowledged that five terms may not be sufficient to accurately represent some highly complex flapping trajectories observed in nature. However, the purpose of this work is not to replicate the flight of a particular insect or bird. The purpose is instead to develop methods to find the optimal instance of a given trajectory structure by assigning numerical values to the trajectory parameters. The number of terms, therefore, was selected (1) to give suitable flexibility to the achievable flapping patterns, and (2) to decrease the parameter space that must be searched by the optimization method. Additional Fourier terms may be added if additional complexity is required.

In each experimental run, high-level MATLAB optimization code running on a PC generates desired flapping trajectories $\theta_{1d}(t)$, $\theta_{2d}(t)$, and $\theta_{3d}(t)$ and sends the trajectories to the controller running on the cRIO. The flapping mechanism executes the trajectories, records the angle and force data from the encoders and strain gages, resolves the forces into the earth-fixed frame, and sends the data to the MATLAB optimization code. The MATLAB code then uses these data to explore the feasible design space and optimize the wing trajectory.

In general, the final angle of a previous trajectory will not match the initial angle of the current trajectory. This occurs as the optimization algorithm selects new parameters in eqn (3). To enable smooth transitions between subsequent trajectories, each DOF is driven from its zero angle to the initial desired trajectory angle using a quintic polynomial trajectory over a period of one second at the beginning of each run. A quintic polynomial ensures a smooth transition into the desired trajectory by matching the angle, angular velocity, and angular acceleration at the transition point [62]. Similarly,

each DOF is driven from its final desired trajectory angle to its zero angle at the end of each run using a quintic polynomial trajectory.

Motor angle commands are calculated from the desired wing angle trajectories using

$$\begin{aligned} Motor_1 &= \theta_1 \\ Motor_2 &= 20\theta_2 + 20\theta_3 \\ Motor_3 &= 20\theta_2 - 20\theta_3 \end{aligned}, \tag{4}$$

where θ_1 is driven directly by the motor, and θ_2 and θ_3 are driven via the differential. In (4) the value of 20 corresponds to the gear ratio of the worm/spear gear set, and sum and difference in the second and third equations arise from the kinematics of the differential. Both shafts must be turned in the same direction to achieve θ_2 motion, thus the sign for θ_2 in both Motor_2 and Motor_3 is positive. Both shafts must be turned in opposite directions to achieve θ_3 motion, thus the signs for θ_3 alternate.

Each experimental run consists of an initial one-second transition from the zero angle configuration, followed by six cycles of the experimental trajectory defined by eqn (3), and a final one-second transition back to the zero angle configuration. To minimize transient effects and to enable signal averaging, the two transition periods and the first period of the desired trajectory are excluded in evaluating the average vertical force [63].

Frequency selection and fluid flow velocity are calculated using Reynolds and Strouhal number scaling. Given an animal length L_{animal}, an animal velocity U_{animal}, and the kinematic viscosity, v_{animal}, the Reynolds number for a flying animal is defined as

$$\text{Re} = \frac{U_{animal} L_{animal}}{v_{animal}} . \tag{5}$$

Given a flapping frequency, f_{animal}, the Strouhal number for a flying animal is defined as

$$St = \frac{L_{animal} f_{animal}}{U_{animal}} . \tag{6}$$

Equating (5) with the Reynolds number for a scaled mechanism and solving for the ratio of the scaled velocity to the animal velocity yields

$$\frac{U_{scale}}{U_{animal}} = \frac{L_{animal} v_{scale}}{L_{scale} v_{animal}} . \tag{7}$$

Equating (6) with the Strouhal number for a scaled mechanism and solving for the ratio of the scaled velocity to the animal velocity yields

$$\frac{U_{scale}}{U_{animal}} = \frac{L_{scale} f_{scale}}{L_{animal} f_{animal}} . \tag{8}$$

Equating eqns (7-8) and solving for f_{scale} yields

$$f_{scale} = \left(\frac{v_{scale}}{v_{animal}} \right) \left(\frac{L_{animal}}{L_{scale}} \right)^2 f_{animal} , \tag{9}$$

where v_{scale} and L_{scale} depend on the experimental setup. For studies involving a ladybug as mentioned here (L_{animal} = 0.008 m, f_{animal} = 80 Hz, v_{animal} = 1.46 x 10^{-5} m^2/s), L_{scale} is 0.14 m, v_{scale} is 1.12 x 10^{-6} m^2/s (kinematic viscosity of water) and f_{scale} is 0.025 Hz [2]. For convenience, however, the fundamental

frequency (f_{scale}) was set to 0.50 Hz to maximize the signal-to-noise ratio. This fundamental frequency enabled the completion of approximately two optimization iterations per minute. In these studies, a wing profile resembling a ladybug wing was used [64]. Wing profiles are made from acrylic measuring about 3 mm thick (0.125 in).

3.2 Optimization Approach

As discussed previously, one of the purposes of the mechanism is to enable experimental optimization of flapping trajectories, which corresponds to finding the optimal Fourier coefficients in eqn (3) from experimental force and motion data. The chosen optimization approach was based on the three-level Box-Behnken screening design to vary the model parameters [65], [66]. In this approach, the Box-Behnken systematically varies the coefficients of the Fourier-series expansion that describe the wing trajectories in eqn (3). This method is an efficient way of exploring a model which may have a large design space. The flapping trajectories corresponding to all combinations of Fourier coefficients are executed, and the optimal lift- or thrust-generating trajectory is identified. Each trajectory was repeated twice to allow comparison of resulting forces for consistency and to quantify experimental uncertainty.

4. RESULTS AND DISCUSSION

4.1 Mechanism Response

To quantify the frequency capabilities of the mechanism, a swept sine wave with an amplitude of 45° and frequency content of 0-5 Hz was input into each DOF of the flapping mechanism using closed-loop control. Each DOF was driven independently with the wing attached. This was performed in both flowing water (u_y = 0.25 m/s) and quiescent air. The closed-loop system response indicated the physical capabilities of the system and its ability to track trajectories at different frequencies. Figure 6 shows the frequency response of the system, plotted as measured amplitude/commanded amplitude, in dB.

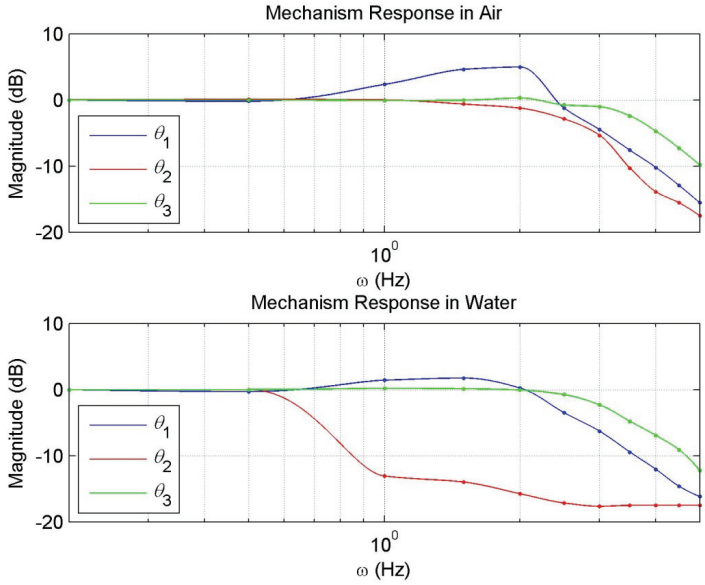

Figure 6. Mechanism frequency response for all DOFs using a swept sine (0-5 Hz) input. The plots show the ratio of the measured trajectory amplitude to the commanded trajectory amplitude.

As seen in Figure 6, the mechanism is capable of tracking all 3 DOFs at low frequencies with little error. Higher frequencies (0.5-1 Hz) did exhibit some trouble tracking in the θ_2 DOF. This caused for some tracking error when the mechanism was attempting to track large-amplitude high-frequency kinematics. Figure 7 shows tracking results for an arbitrary flapping pattern near the frequencies of interest for the mechanism flapping in water flowing at 0.25 m/s. In the figure, $\theta_1 - \theta_3$ are the recorded angles of each DOF and $\theta_{1d} - \theta_{3d}$ are the desired (commanded) angles of each DOF. As seen in the figure, there is a high tracking accuracy at this frequency.

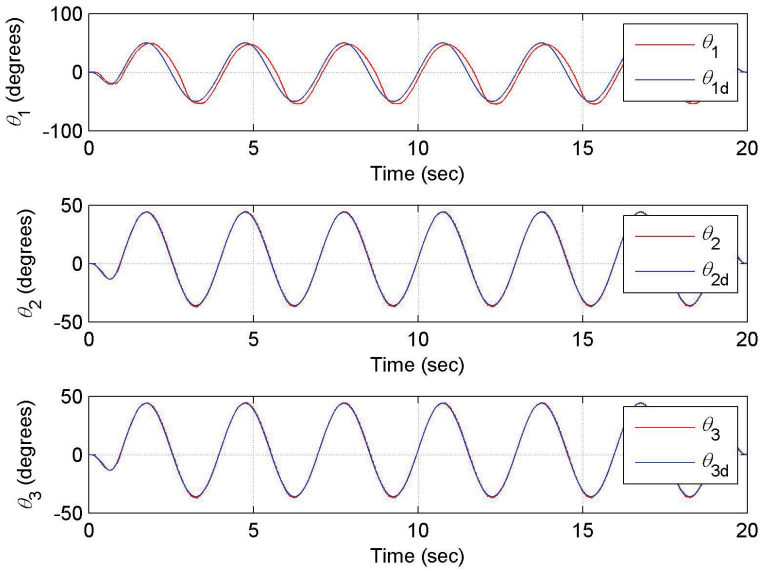

Figure 7. Tracking results of an arbitrary flapping trajectory. $\theta_1 - \theta_3$ are the recorded angles of each DOF and $\theta_{1d} - \theta_{3d}$ are the desired (commanded) angles of each DOF.

4.2 Lift and Thrust Production

To verify the optimization approach and demonstrate the suitability of the flapping mechanism, a preliminary optimization run was performed using a ladybug wing shape (see Figure 8) [64]. The flume water velocity was 0.25 m/s. The Box-Behnken screening design (consisting of 432 runs) was performed twice for the starting trajectory (A) and step sizes defined in Table 2. In this table B corresponds to the trajectory that maximized thrust with neutral lift, C corresponds to the trajectory that maximized lift with neutral thrust, and D corresponds to the trajectory that maximized both lift and thrust. Figure 9 shows average lift vs. average thrust for each run. The Box-Behnken design identified trajectories with improved thrust of 4.55 units and lift of 2.64 units relative to the starting trajectories, suggesting the feasibility of the proposed optimization approach and the suitability of the mechanism.

Table 2. Step size for Box-Behnken testing and trajectories for runs labeled in Figure 9. Bold values indicate a deviation from the starting trajectory (A).

	Step Size (°)	A (°)	B (°)	C (°)	D (°)
A_{11}	24	0	0	0	0
A_{12}	32	50	50	50	50
A_{13}	32	0	0	0	0
A_{14}	32	0	0	0	0
A_{15}	32	0	**-32**	**32**	**-32**
A_{21}	24	-20	-20	**4**	-20
A_{22}	32	40	40	40	**72**
A_{23}	32	0	0	0	0
A_{24}	32	0	0	0	0
A_{25}	32	0	0	0	0
A_{31}	24	0	**24**	0	0
A_{32}	32	0	0	0	0
A_{33}	32	45	45	45	45
A_{34}	32	0	0	0	0
A_{35}	32	0	0	0	0

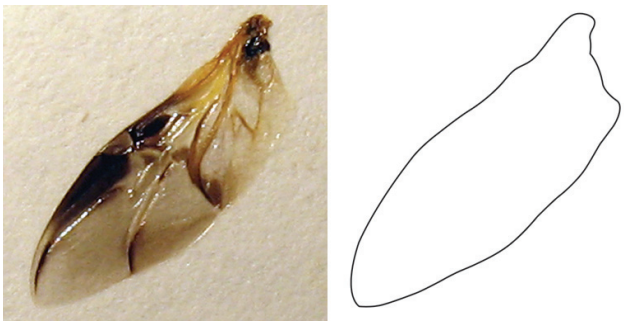

Figure 8. Ladybug wing and outline used for acrylic wing fabrication.

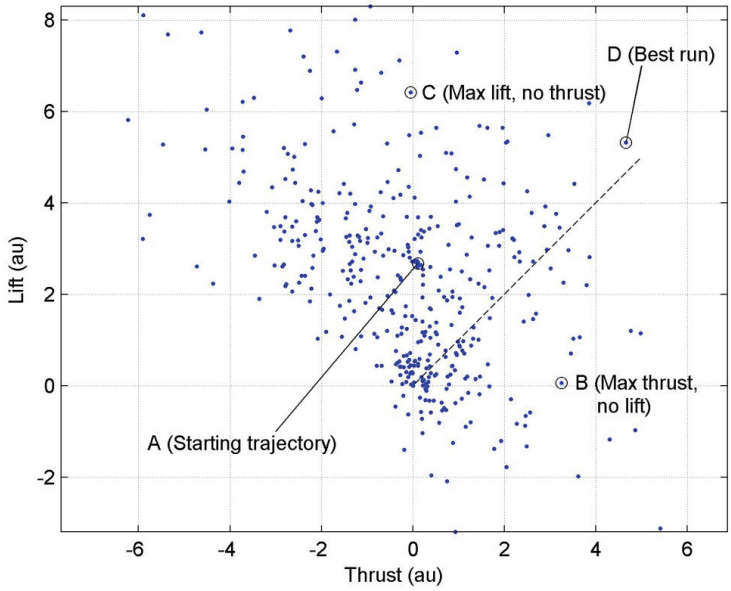

Figure 9. Lift and thrust values averaged from two identical Box-Behnken iterations (432 runs performed twice). The dashed line represents the direction of the desired force, assuming equal priority for thrust and lift.

Figure 10 represents the starting trajectory (A) identified in Figure 9. This trajectory was chosen to maximize the search area of the Box-Behnken screening design for the chosen step size. The force history shows positive lift and neutral thrust. Figure 11 represents the trajectory exhibiting the maximum thrust with neutral lift (B). The optimization accomplished this by adjusting the rotation angle (θ_1) and the feathering angle (θ_3). The force history shows wholly positive thrust and neutral lift. Figure 12 represents the trajectory exhibiting the maximum lift with neutral thrust (C). The optimization accomplished this by adjusting the rotation angle (θ_1) and the elevation angle (θ_2). The force history shows two strong positive peaks of lift and neutral thrust. Figure 13 represents the trajectory considered to be the best run (D). This was chosen by the run that was furthest out in the search direction (dashed line in Figure 9) and within a reasonable tolerance of the line. The optimization accomplished this by adjusting the rotation angle (θ_1) and the elevation angle (θ_2). The force history shows strong lift and thrust peaks generated in phase with each other with small, less significant peaks between.

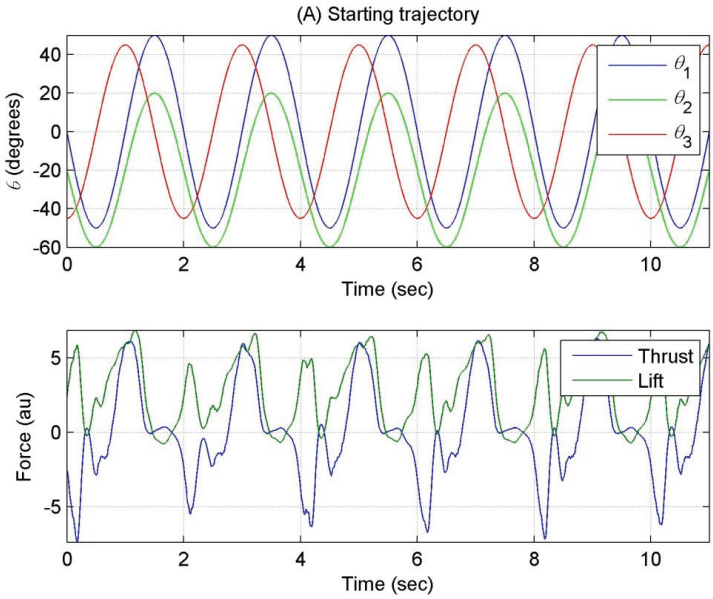

Figure 10. Force and trajectory history for (A) starting trajectory.

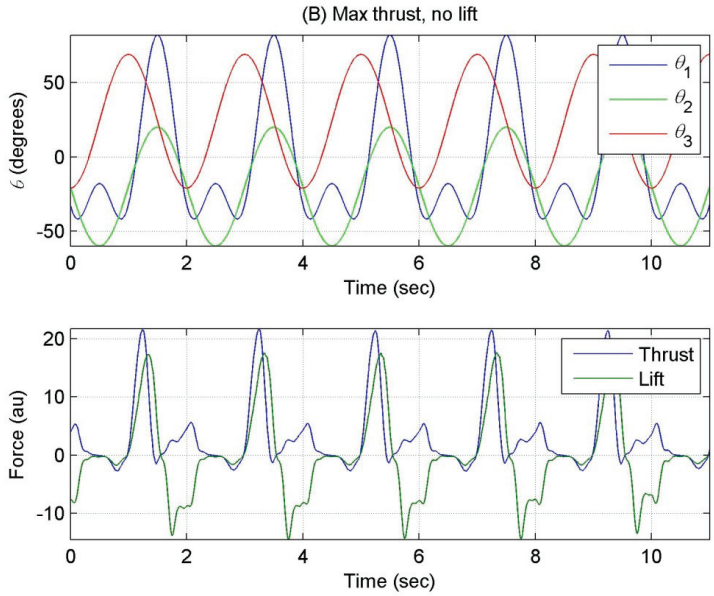

Figure 11. Force and trajectory history for (B) max thrust, no lift.

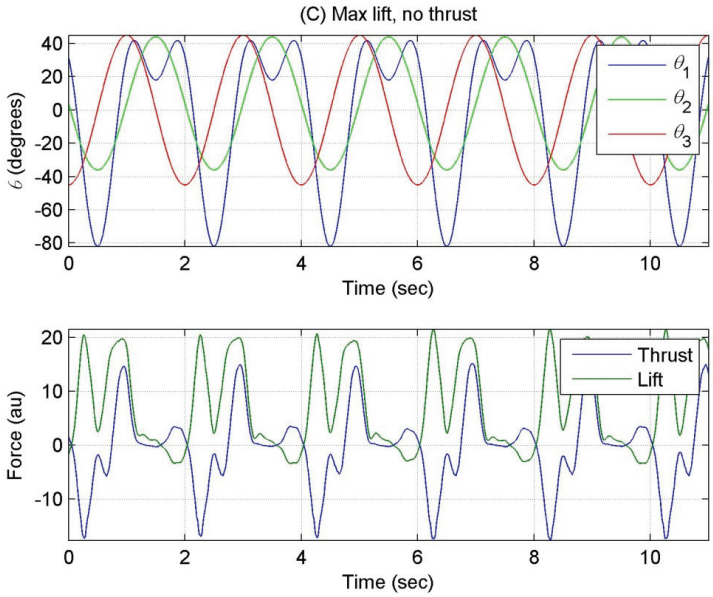

Figure 12. Force and trajectory history for (C) max lift, no thrust.

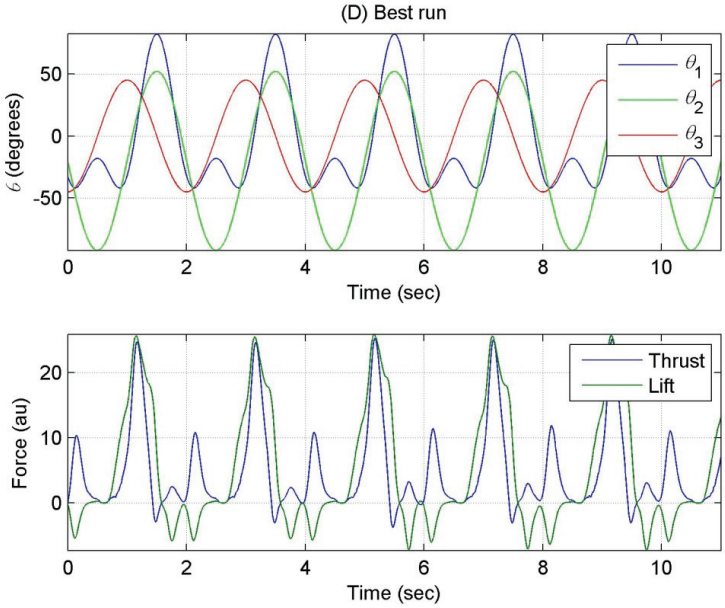

Figure 13. Force and trajectory history for (D) best run.

Figure 14 contains force magnitude outputs for both Box-Behnken design runs (432 runs performed two times). The data follow a linear trend showing consistency in the measurements. Runs that deviate from the dotted line are runs that did not track the commanded trajectory consistently between iterations.

Figure 15 shows the unresolved force output for a single arbitrary trajectory. This trajectory was run 24 times (12 consecutive runs performed twice). Resulting force output is plotted, again showing consistency in the data. Figure 16 shows ensemble averaged force output from 24 runs.

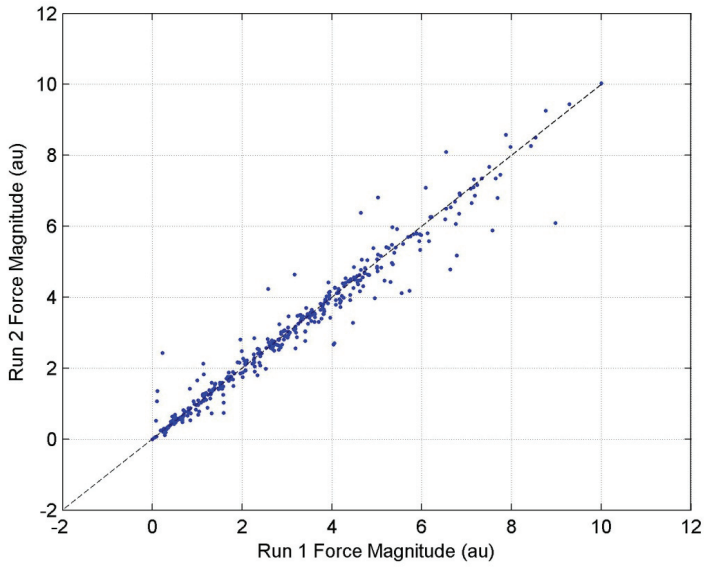

Figure 14. Force magnitude outputs compared over two iterations.

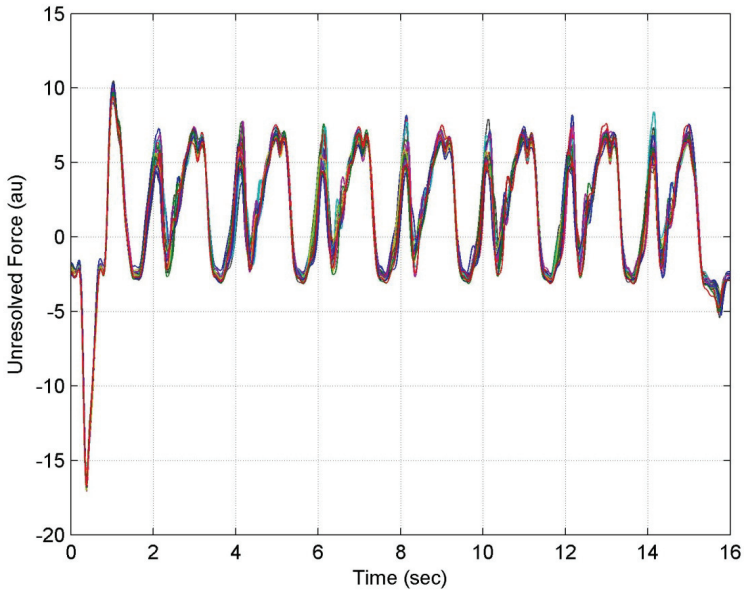

Figure 15. Force output for an arbitrary flapping trajectory performed 24 times.

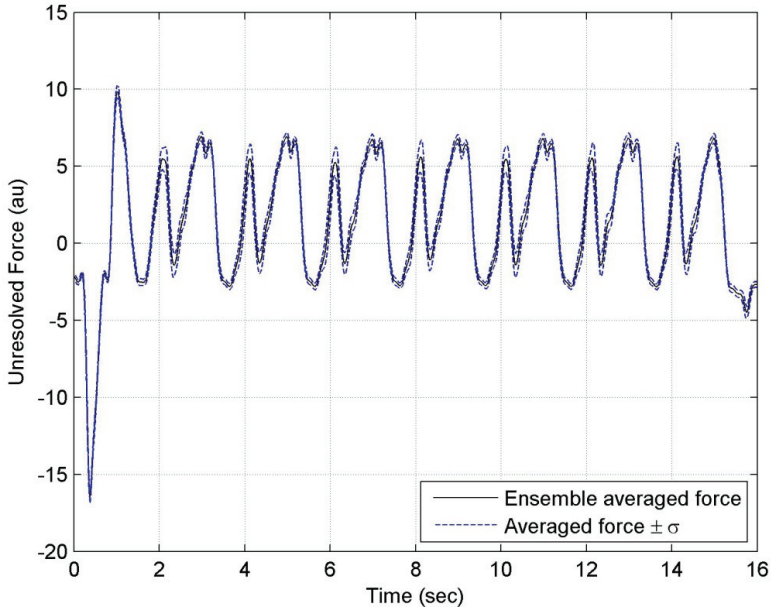

Figure 16. Ensemble-averaged force output, along with standard deviation, of 24 runs.

4.3 Force Uncertainty

The main contributing factors to uncertainty in the measurements are (1) noise in the raw data signal from the strain gages, (2) position error due to encoder resolution, and (3) position error due to gear backlash. The latter is quantified by comparing differences in force output from identical runs. The error due to noise in the strain gages is estimated by

$$u_{0,noise} = \pm\frac{1}{2}\left[0.218\ au\right]. \tag{10}$$

The error due to the resolution of the encoders was estimated by finding the change in force output due to a change in the motor position. This motor position was defined by the minimum change in angle that the encoder is capable of measuring (θ_1=0.119°, θ_2=θ_3=0.176°). The error, $u_{\text{resolution}}$, due to the encoder resolution was 0.0148 au.

The error due to backlash present in the differential gears was estimated by measuring the backlash of each DOF (θ_1=0.5°, θ_2=4°, θ_3=2°) and finding the resulting change in the force output due to the change in position from the gear backlash. The total error due to backlash present in the differential gears was u_{backlash} = 0.1377 au.

The total force output uncertainty is estimated by

$$u_{total} = \pm\sqrt{\left(u_{0,noise}^2 + u_{resolution}^2 + u_{backlash}^2\right)}\ , \tag{11}$$

with a numerical value of u_{total} = ±0.176 au. For the force values presented in this study, this uncertainty value accounts for 6% or less of the total force output.

CONCLUSION

This paper describes a two-wing mechanism for laboratory flapping flight experiments. Each wing is capable of three DOFs of motion, with two of the DOFs achieved using a differential gear design and the third DOF being achieved through a rotating turntable. Each wing is driven by three brushless motors and is capable of accurately tracking trajectories from 0-0.5 Hz in water and 0-1 Hz in air. The

mechanism has adjustable kinematics, is capable of flapping in harsh environments (e.g., underwater), and can measure flapping force and angles in real time. Additionally, two wings sit back to back, allowing the experimental investigation of the effects of clap-and-fling and other flapping phenomena.

An experimental approach to finding the optimal lift- and thrust-generating flapping trajectories was also presented. The method, based on the Box-Behnken approach to exploring the design space, finds the trajectory parameters (in this case, Fourier coefficients) that result in trajectories that exhibit maximum thrust and/or lift. The method was demonstrated using a wing based on that of a lady bug. The Box-Behnken design method found a trajectory that improved lift and thrust by 2.64 and 4.55 units, respectively, indicating that the approach has the potential to increase the effectiveness of flapping flight. The uncertainty in the force measurements was found to be ±0.176 units. The results obtained in this work demonstrate that the mechanism is a capable test bed for further optimization of kinematic trajectories and force analysis.

Future work will make use of the system described in this paper to explore the role of flapping trajectories on lift and thrust generation. Different animal scaling parameters will be used to allow the mechanism to be properly scaled and still maintain a high signal-to-noise ratio. Of particular interest are the flapping dynamics of a zebra finch and intermittent flight. The role of the leading edge vortex will also be explored with particle image velocimetry.

ACKNOWLEDGEMENTS

This work is supported by the Air Force Office of Scientific Research award FA9550-10-1-0334. The authors gratefully acknowledge the contribution of Kevin Cole and members of the Flapping Flight Research Group at Brigham Young University.

REFERENCES

[1] Mathew A Camper, "An Insect's Role in the Development of Micro Air Vehicles," Colorado State University, Fort Collins, CO.

[2] Wei Shyy, Yongsheng Lian, Jian Tang, Dragos Viieru, and Hao Liu, *Aerodynamics of Low Reynolds Number Flyers*. Cambridge: Cambridge University Press, 2008.

[3] Michael J C Smith, "Simulating Moth Wing Aerodynamics: Towards the Development of Flapping-Wing Technology," *AIAA Journal*, vol. 34, pp. 1348-1355, 1996.

[4] Michael J C Smith, "Wing-Drive Mechanism, Vechicle Employing Same, and Method for Controlling the Wing-Drive Mechanism and Vehicle Employing Same," Hardware 6206324, March 27, 2001.

[5] Coen VandenBerg and Charles P Ellington, "The three-dimensional leading-edge vortex of a 'hovering' model hawkmoth," *Philosophical Transactions: Biological Sciences*, vol. 352, no. 1351, pp. 329-340, 1997.

[6] C P Ellington, "The Novel Aerodynamics of Insect Flight: Applications to Micro-air Vehicles," *The Journal of Experimental Biology*, vol. 202, pp. 3439-3448, 1999.

[7] Michael H Dickinson, Fritz-Olaf Lehmann, and Sanjay P Sane, "Wing Rotation and the Aerodynamic Basis of Insect Flight," *Science*, vol. 284, pp. 1954-1960, June 1999.

[8] R S Fearing et al., "Wing Transmission for a Micromechanical Flying Insect," in *International Conference on Robotics and Automation*, San Francisco, CA, 2000, pp. 1509-1516.

[9] Metin Sitti, "PZT Actuated Four-Bar Mechanism with Two Flexible Links for Micromechanical Flying Insect Thorax," in *IEEE International Conference on Robotics and Automation*, 2001, pp. 3893-3900.

[10] K D Frampton and M Goldfarb, "Passive Aeroelastic Tailoring for Optimal Flapping Wings," in *Conference on Fixed, Flapping and Rotary Winged Vehicles for Very Low Reynolds Numbers*, Notre Dame, IN, 2000.

[11] T Pornsin-Sisirak et al., "MEMS Wing Technology for a Battery-Powered Ornithopter," in *13th IEEE International Conference on Micro Electro Mechanical Systems*, Miyazaki, Japan, 2000, pp. 799-804.

[12] J Yan, R J Wood, and Z A, Agrawal, S K Khan, "Towards Flapping Wing Control for a Micromechanical Flying Insect," in *IEEE International Conference on Robotics and Automation*, New York, NY, 2001, pp. 3901-3908.

[13] Adam Cox, Daniel Monopoli, Dragan Cveticanin, Michael Goldfarb, and Ephrahim Garcia, "The Development of Elastodynamic Components for Piezoelectrically Actuated Flapping Micro-air Vehicles," *Journal of Intelligent Material Systems and Structures*, vol. 13, pp. 611-615, September 2002.

[14] S Avadhanula, R J Wood, E Steltz, J Yan, and R S Fearing, "Lift Force Improvements for the Micromechanical Flying Insect," in *IEEE International Conference on Intelligent Robotics and Systems*, Las Vegas, NV, 2003, pp. 1350-1356.

[15] Joseph Yan and Ronald Fearing, "Wing Force Map Characterization and Simulation for the Micromechanical Flying Insect," in *IEEE International Conference on Intelligent Robots and Systems*, Las Vegas, NV, 2003, pp. 1343-1349.

[16] David L Raney and Eric C Slominski, "Mechanization and Control Concepts for Biologically Inspired Micro Aerial Vehicles," in *AIAA Guidance, Navigation & Control Conference*, Austin, TX, 2003, pp. 1-11.

[17] M J Tarascio and I Chopra, "Design and Development of a Thrust Augmented Entomopter: An Advanced Flapping Wing Micro Hovering Air Vehicle," in *59th Annual Forum of the American Helicopter Society*, Phoenix, AZ, 2003.

[18] Beerinder Singh, Manikandan Ramasamy, Inderjit Chopra, and J Gordon Leishman, "Experimental Studies on Insect-Based Flapping Wings for Micro Hovering Air Vehicles," *AIAA Journal*, vol. 46, pp. 2115-2135, 2008.

[19] S C Burgess, K Alemzadeh, and L Zhang, "The development of a miniature mechanism for producing insect wing motion," *Design and Nature II*, pp. 237-244, 2004.

[20] Nilesh D Mankame and G K Ananthasuresh, "A Novel Compliant Mechanism for Converting Reciprocating Translation Into Enclosing Curved Paths," *Journal of Mechanical Design*, vol. 126, pp. 667-672, July 2004.

[21] Will J Maybury and Fritz-Olaf Lehmann, "The fluid dynamics of flight control by kinematic phase lag variation between two robotic insect wings," *The Journal of Experimental Biology*, vol. 207, pp. 4707-4726, 2004.

[22] Adrian L R Thomas, Graham K Taylor, Robert B Srygley, Robert L Nudds, and Richard J Bomphrey, "Dragonfly flight: free-flight and tethered flow visualizations reveal a diverse array of unsteady lift-generating mechanisms, controlled primarily via angle of attack," *The Journal of Experimental Biology*, vol. 207, pp. 4299-4323, 2004.

[23] Sai K Banala and Sunil K Agrawal, "Design and Optimization of a Mechanism for Out-of-Plane Insect Winglike Motion With Twist," *Journal of Mechanical Design*, vol. 127, no. 4, pp. 841-844, 2005.

[24] Cezary Galinski and Rafa? Zbikowski, "Insect-like flapping wing mechanism based on a double spherical Scotch yoke," *J. R. Soc. Interface*, vol. 2, pp. 223-235, 2005.

[25] Rafał Zbikowski, Cezary Galinski, and Christopher B Pedersen, "Four-Bar Linkage Mechanism for Insectlike Flapping Wings in Hover: Concept and an Outline of Its Realization," *Journal of Mechanical Design*, vol. 127, pp. 817-824, July 2005.

[26] Winson Lai, Joseph Yan, Mehran Motamed, and Sheldon Green, "Force Measurements on a Scaled Mechanical Model of Dragonfly in Forward Flight," in *International Conference on Advanced Robotics*, 2005, pp. 595-600.

[27] Rajkiran Madangopal, Zaeem A Khan, and Sunil K Agrawal, "Biologically Inspired Design of Small Flapping Wing Air Vehicles Using Four-Bar Mechanisms and Quasi-steady Aerodynamics," *Journal of Mechanical Design*, vol. 127, pp. 809-816, July 2005.

[28] Rajkiran Madangopal, Zaeem Ashraf Khan, and Sunil K Agrawal, "Energetics-Based Design of Small Flapping-Wing Micro Air Vehicles," *IEEE/ASME Transactions on Mechatronics*, vol. 11, no. 4, pp. 433-438, 2006.

[29] Sean H McIntosh, Sunil K Agrawal, and Zaeem Khan, "Design of a Mechanism for Biaxial Rotation of a Wing for a Hovering Vehicle," in *IEEE/ASME Transaction of Mechatronics*, 2006, pp. 145-153.

[30] Sunil K Agrawal, Sean H McIntosh, and Zaeem Khan, "Mechanism for Biaxial Rotation of a Wing and Vehicle Containing Such Mechanism," Hardware 7651051, January 26, 2010.

[31] Hiroto Tanaka, Kazunori Hoshino, Kiyoshi Matsumoto, and Isao Shimoyama, "Flight Dynamics of a Butterfly-type Ornithopter," in *International Conference on Intelligent Robots and Systems*, 2005, pp. 2706-2711.

[32] M Yamamoto and K Isogai, "Measurement of unsteady fluid dynamic forces for a mechanical dragonfly model," *AIAA Journal*, vol. 43, no. 12, 2005.

[33] Andrew Conn, Stuart Burgess, Rick Hyde, and Seng Ling, "From Natural Flyers to the Mechanical Realization of a Flapping Wing Micro Air Vehicle," in *International Conference on Robotics and Biomimetics*, Kunming, China, 2006, pp. 439-444.

[34] A T Conn, S C Burgess, and Ling C S, "Design of a parallel crank-rocker flapping mechanism for insect-inspired micro air vehicles," *Journal of Mechanical Engineering Science*, vol. 221, pp. 1211-1222, 2007.

[35] K M Isaac, "Force Measurements on a Flapping and Pitching Wing at Low Reynolds Numbers," in *44th AIAA Aerospace Sciences Meeting*, Reno, NV, 2006, pp. 1-14.

[36] Moh Syaifuddin, Hoon Cheol Park, and Nam Seo Goo, "Design and evaluation of a LIPCA-actuated flapping device," *Smart Materials and Structures*, vol. 15, pp. 1225-1230, 2006.

[37] Viet-Quoc Nguyen et al., "Characteristics of an Insect-mimicking Flapping System Actuated by a Unimorph Piezoceramic Actuator," *Journal of Intelligent Material Systems and Structures*, vol. 00, pp. 1-9, 2008.

[38] Christopher DiLeo and Xinyan Deng, "Experimental Testbed and Prototype Development for a Dragonfly-Inspired Robot," in *Conference on Intelligent Robots and Systems*, San Diego, CA, 2007, pp. 1594-1599.

[39] Zaeem A Khan and Sunil K Agrawal, "Design and Optimization of a Biologically Inspired Flapping Mechanism for Flapping Wing Micro Air Vehicles," in *IEEE International Conference on Robotics and Automation*, Roma, Italy, 2007, pp. 373-378.

[40] R J Wood, "Design, fabrication, and analysis of a 3DOF, 3cm flapping-wing MAV," in *IEEE International Conference on Intelligent Robots and Systems*, San Diego, CA, 2007, pp. 1576-1581.

[41] Lung-Jieh Yang, Cheng-Kuei Hsu, Jen-Yang Ho, and Chao-Kang Feng, "Flapping wings with PVDF sensors to modify the aerodynamic forces of a micro air vehicle," *Sensors and Actuators*, vol. 139, pp. 95-103, 2007.

[42] G Bunget and S Seelecke, "BATMAV: a biologically-inspired micro-air vehicle for flapping flight: kinematics and actuation," in *Proceedings of SPIE*, 2008.

[43] Ch Grand, P Martinelli, J B Mouret, and S Doncieux, "Flapping-Wing Mechanism for a Bird-Sized UAVs: Design, Modeling and Control," *Advances in Robot Kinematics: Analysis and Design*, pp. 127-134, 2008.

[44] David Lentink, Florian T Muijres, Frits Donker-Duyvis, and Johan L van Leeuwen, "Vortex-wake interactions of a flapping foil that models animal swimming and flight," *The Journal of Experimental Biology*, vol. 211, pp. 267-273, 2008.

[45] Jonathan Maglasang, Norihiro Goto, and Koji Isogai, "Development of Bird-like Micro Aerial Vehicle with Flapping and Feathering Wing Motions," *Trans. Japan Soc. Aero. Space Sci.*, vol. 51, no. 171, pp. 8-15, 2008.

[46] Hiroto Nagai, Koji Isogai, and Toshiyuki Hayase, "Measurement of Unsteady Aerodynamic Forces of 3D Flapping Wing in Hovering to Forward Flight," in *26th International Congress of the Aeronautical Sciences*, 2008, pp. 1-11.

[47] Joon Hyuk Park and Kwang-Joon Yoon, "Designing a Biomimetic Ornithopter Capable of Sustained and Controlled Flight," *Journal of Bionic Engineering*, vol. 5, no. 1, pp. 39-47, 2008.

[48] Wojciech Bejgerowski, Arvind Ananthanarayanan, Dominik Mueller, and Satyandra K Gupta, "Integrated Product and Process Design for a Flapping Wing Drive Mechanism," *Journal of Mechanical Design*, vol. 131, June 2009.

[49] C T Bolsman, J F L Goosen, and F van Keulen, "Design Overview of a Resonant Wing Actuation Mechanism for Application in Flapping Wing MAVs," *International Journal of Micro Air Vehicles*, vol. 1, no. 4, pp. 263-272, 2009.

[50] Benjamin M Finio, Brandon Eum, Christopher Oland, and Robert J Wood, "Asymmetric flapping for a robotic fly using a hybrid power-control actuator," in *Proceedings of the 2009 IEEE/RSJ international conference on Intelligent robots and systems*, St. Louis, MO, 2009, pp. 2755—2762.

[51] Tatjana Y Hubel and Cameron Tropea, "Experimental investigation of a flapping wing model," *Experiments in Fluids*, vol. 46, pp. 945-961, 2009.

[52] Roman Y Krashanitsa, Dmitro Silin, and Sergey V Shkarayev, "Flight Dynamics of a Flapping-Wing Air Vehicle," *International Journal of Micro Air Vehicles*, vol. 1, no. 1, pp. 35-49, 2009.

[53] Kevin Massey, Ashley Flick, and Gautam Jadhav, "Force Measurements and Flow Visualization for a Flexible Flapping Wing Mechanism," *International Journal of Micro Air Vehicles*, vol. 1, no. 3, pp. 183-202, November 2009.

[54] Scott L Thomson et al., "Experiment-Based Optimization of Flapping Wing Kinematics," in *47th AIAA Aerospace Sciences Meeting*, Orlando, FL, 2009, pp. 1-8.

[55] Bor-Jang Tsai and Yu-Chun Fu, "Design and aerodynamic analysis of a flapping-wing micro air vehicle," *Aerospace Science and Techology*, vol. 13, pp. 383-392, 2009.

[56] Michael A A Fenelon and Tomonari Furukawa, "Design of an active flapping wing mechanism and a micro aerial vehicle using a rotary acuator," *Mechanism and Machine Theory*, vol. 45, pp. 137-146, 2010.

[57] Jong-seob Han and Jo Won Chang, "Flow Visualization and Force Measurement of an Insect-based Flapping Wing," in *48th AIAA Aerospace Sciences Meeting*, Orlando, FL, 2010, pp. 1-10.

[58] Sujoy Mukherjee and Ranjan Ganguli, "Non-linear Dynamic Analysis of a Piezoelectrically Actuated Flapping Wing," *Journal of Intelligent Material Systems and Structures*, vol. 21, pp. 1157-1167, August 2010.

[59] R B Dryburgh, B G W Peter, and W G Plewes, "Waterproofing Strain Gages on Reinforcing Bars in Contrete Exposed to the Sea," *American Society for Testing and Materials - Materials Research and Standards*, vol. 5, no. 7, pp. 350-351, August 1965.

[60] Hikaru Aono, Wei Shyy, and Hao Lui, "Near wake vortex dynamics of a hovering hawkmoth," *Acta Mech Sin*, vol. 25, pp. 23-36, 2009.

[61] W Shyy et al., "Recent progress in flapping wing aerodynamics and aeroelasticity," *Progress in Aerospace Sciences*, vol. 46, pp. 284-327, 2010.

[62] John J Craig, *Introduction to Robotics: Mechanics and Control*, 3rd ed.: Prentice Hall, 2004.

[63] J M Birch and M H Dickinson, "Spanwise flow and the attachment of the leading-edge vortex on insect wings," *Nature*, vol. 412, pp. 729-733, 2001.

[64] Ryan B George and Scott L Thomson, "High-Speed, Three-Dimensional Quantification of Ladybug (Hippodamia convergens) Flapping Wing Kinematics During Takeoff," in *48th AIAA Aerospace Sciences Meeting*, Orlando, FL, 2010, pp. 1-11.

[65] G E P Box and D W Behnken, "Some New Three Level Designs for the Study of Quantitative Variables," *Technometrics*, vol. 2, no. 4, pp. 455-475, November 1960.

[66] S L C Ferreira et al., "Box-Behnken design: An alternative for the optimization of analytical methods," *Analytica Chimica Acta*, vol. 597, pp. 179-186, 2007.